Functionalization of Carbon Nanotubes by Ammonia Glow-Discharge: Experiments and Modeling

Bishun N. Khare,* Patrick Wilhite, Richard C. Quinn, Bin Chen, Robert H. Schingler, Benjamin Tran, Hiroshi Imanaka, Christopher R. So, Charles W. Bauschlicher, Jr.,* and M. Meyyappan

Center for Nanotechnology, NASA Ames Research Center, Moffett Field, California 94035

Received: February 12, 2004; In Final Form: April 20, 2004

We successfully functionalized single-walled carbon nanotubes (SWNTs) through a microwave discharge of ammonia. Evidence is supplied through Fourier transform infrared (FTIR) spectroscopy with band assignment aided by computational modeling. X-ray photoelectron spectroscopy (XPS) and Raman spectroscopy results also provide supporting evidence of functional groups attached to the surfaces of SWNTs from ammonia plasma.

I. Introduction

There is considerable interest in functionalizing carbon nanotubes (CNTs) for several applications. By adding species to the side walls, the electrical and/or mechanical properties can be altered. Typically, such functionalization is accomplished by immersing the nanotubes in appropriate chemical solutions or exposing them to vapors at high temperatures. As an alternative, it was shown recently that H atoms could be added to carbon nanotubes using a cold plasma approach.[1,2] The cold plasma approach is not limited to H atoms but rather offers a simple technique for adding a variety of atomic and molecular radicals to the side walls. In this work we describe functionalization using NH_3 as a precursor, which is expected to yield H, N, NH, and NH_2 radicals, all of which are able to bond to the nanotube walls. To aid in the identification of the experimental products and contribute to an understanding of which products are formed, we also report the results of ab initio calculations. FTIR, Raman spectroscopy, and X-ray photoelectron spectroscopy (XPS) have been used to characterize the functionalized samples.

II. Experiment

Preparation and purification of HiPCO-derived single-wall carbon nanotubes (SWNT) are described elsewhere.[1] SWNTs suspended in 2-propanol solution were deposited on CaF_2 disks (25 mm by 4 mm) and were subsequently heated to 650 °C to remove solvent impurities. Spectra taken with a Thermo-Nicolet Nexus 670 FTIR spectrometer show that no new bands appear after heating the SWNTs. The bands corresponding to C−H stretching were still present after baking, though significantly reduced. Thus, we believe that we have reduced, but not completely eliminated, some hydrocarbon impurities. As we later illustrate, some of our products are consistent with residual hydrocarbons. The sample used in the XPS analysis was more densely coated and separated from the CaF_2 substrate. After heating, it was cut to make two "bucky films" with one used as a control and the other used for functionalization.

A microwave discharge was used to generate the ammonia plasma. The source consists of a Pyrex tube (inner diameter of 10 mm and 1 mm thickness) inserted into a McCarroll cavity operated at 2.45 GHz (see Figure 1). Microwave power was supplied by an Opthos microwave generator (model MPG-4M). The net delivered power was kept around 100 W. The setup previously used for functionalization[1,2] proved inadequate; preliminary discharges showed that the overall path length from the discharge tube to the sample had to be reduced to enable the plasma species to impact the target before recombining to lower energetic states. During a typical run, a SWNT sample was inserted and held in position inside a 1 in. Cajon Ultra-Torr type vacuum fitting (Figure 1). By omitting the chamber used in earlier work, we reduced the overall path length from roughly 7 cm to 1 cm. The corresponding opening of the Ultra-Torr fitting was connected directly to the discharge and separated from the sample by a Teflon plug, while the exit end of the tube was connected to a vacuum. This Teflon plug has a 2 mm bore down the center that collimates the plasma species streaming toward the target. To prevent UV radiation from hitting the sample, the entrance hole of the Teflon plug is designed off-axis, enabling only plasma species to pass and strike the target. Further details of the experimental setup can be found in refs 1 and 2. The pressure of the gas leading to the discharge cavity was maintained at approximately 180 mTorr, while the exit end was at approximately 10^{-2} mTorr. Functionalization runs were performed for 20, 40, and, in the case of deuterated ammonia, 210 min. An RF inductively coupled plasma operated from 25 to 100 W of delivered power was also used in initial experiments, and a brief discussion is provided in Experimental Results and Discussion of this paper.

Several calibration experiments were performed. In the first set, experiments were performed without turning on the discharge. In this configuration, no IR bands were observed for time periods well exceeding 3 h. In a second test, a 40 min NH_3 discharge was performed on a CaF_2 disk containing previously deposited 2-propanol (solvent), but no SWNTs. The disk was heated to 650 °C, and no IR bands were observed after the discharge.

X-ray photoelectron spectroscopy analysis of the nanotube samples—both control and plasma-exposed—was carried out

* To whom correspondence should be addressed. E-mails: bkhare@mail.arc.nasa.gov (B.N.K.); charles.w.bauschlicher@nasa.gov (C.W.B.).

10.1021/jp049359q CCC: $27.50
Published on Web 05/25/2004

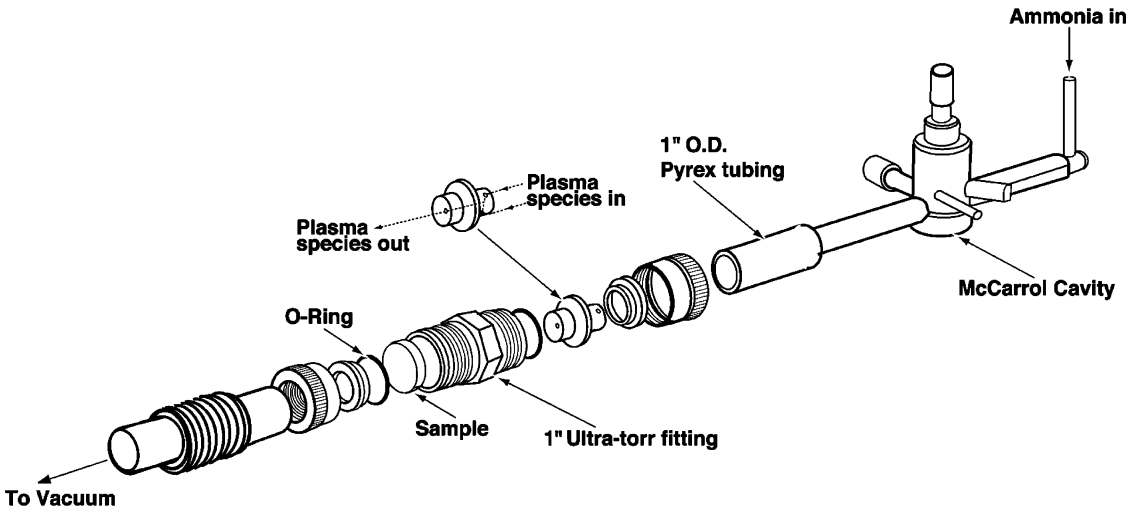

Figure 1. Schematic figure of the experimental setup used to functionalize SWNT.

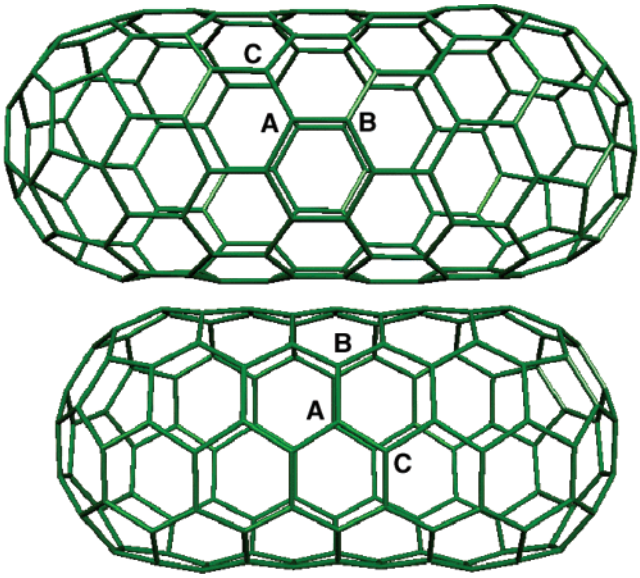

Figure 2. (9,0) and (5,5) tubes used in the computational modeling.

using a HP 5950 ESCA spectrometer. The instrument employs a monochromatic Al-*k* source and was operated at a power of 600 W. The integrated sampling depth was 20−40 Å. A survey scan from 0 to 1000 eV was performed, and high-resolution scans for the C, N, and O core regions were obtained. A set of 500 scans was obtained and averaged for each region. Atomic percent compositions were calculated using Gaussian/Lorentzian line shapes for curve fitting (after baseline subtraction) and sensitivity factors incorporated in the HP 5950 system software.

A 785 nm diode laser was used in the Raman spectroscopy analysis of the samples. A 1800 lines/mm grating was used for the optimized throughput as well as resolution for the excitation. A set of double-notch filters was used to block the laser Rayleigh scattering. The spectra resolution is better than 4 cm^{-1} in the 100−4000 cm^{-1} spectral window. Most representative spectra are chosen for presentation here though the entire sample area was probed at each excitation.

III. Computational Model and Methods

We consider (5,5) and (9,0) tubes, which are approximately 10 Å long. Their ends are capped with half of a C_{60} buckyball, yielding C_{130} and C_{150} for the (5,5) and (9,0) tubes, respectively. The tubes are shown in Figure 2. The H, NH, and NH_2 fragments are bonded to the side walls of the tube, not to the caps. When two species are bonded to the tube on adjacent carbons, there are two orientations for each tube. For the (9,0) tube, the two possibilities use atoms A and B or A and C (Figure 2); we denote these two cases as horizontal and diagonal, respectively. The sites for the (5,5) tube are denoted as vertical (A−B) or diagonal (A−C).

The geometries are fully optimized using the two-level ONIOM approach.[3] The hybrid[4] B3LYP[5] functional in conjunction with the 6-31G basis set[6] is used for the high-level treatment, which is applied to 24 tube carbons, the atoms or molecules bonded to the nanotube, and the 12 link hydrogen atoms. The universal force field[7] (UFF) is used for low-level treatment. The vibrational frequencies are computed using the ONIOM approach. To obtain the IR intensities, we perform a B3LYP/6-31G calculation on free $C_{24}H_{12}$ + side wall species, which is constrained to have the geometry from the ONIOM calculation. The difference between the ONIOM and $C_{24}H_{12}$ models is a maximum of 4 cm^{-1} for the N−H stretches and the H−N−H bend. The results for the NH_2 wag differ by up to 30 cm^{-1}. The good agreement between the two models is consistent with the modes being localized on the side group. For the remaining bands, the two models can differ significantly, and an inspection of these modes shows significant motion of the ring carbons or the H link atom motions. Since these modes are not well described in our model, they are not reported. All calculations are performed using Gaussian 98.[8] We identify the modes using Molekel.[9]

IV. Computational Results

As is well-known, the frequencies computed at the present level of theory need to be scaled before comparing with experiment. On the basis of calibration calculations,[10] the C−H stretches should be scaled by 0.958. We establish the best scale factor for the N−H systems by comparing the results of calculations with experiment for NH_3, NH_2, and NH (Table 1). The scale factors are not the same for the NH_n species. Theory is too large for NH_3 but too small for NH, while the error for NH_2 is between these two. It appears that the error in theory varies with the number of open-shell orbitals on the N atoms. Since our chemisorbed species have no open-shell N orbitals, we take the scale factors from NH_3. For N−H stretches, we take 0.923, which is the average of symmetric and asymmetric stretches in NH_3. For the H−N−H bend, we take 0.968, the value found for NH_3. We do not scale the NH_2 wag, since we have no reliable calibration for this mode.

TABLE 1: Summary of the Computed Vibrational Frequencies (cm^{-1}) and IR Intensities (km/mol) for Gas-Phase NH_n

molecule	N−H s-stretch	N−H a-stretch	H−N−H bend
NH			
ω_e	3102		
expt	3282		
scale factor	1.058		
intensity	83.88		
NH_2			
ω_e	3230	3357	1544
expt	3219	3301	1497
scale factor	0.997	0.983	0.970
intensity	45.11	25.35	7.55
NH_3			
ω_e	3576	3776	1680
expt	3337	3444	1627
scale factor	0.933	0.912	0.968
intensity	0.06	13.74	82.85

TABLE 2: Summary of the Computed Vibrational Frequencies (cm^{-1}) and IR Intensities (km/mol) for Two H Atoms on the Tube

(5,5) Tube		
H_2 vertical		
ω_e	2928	2891
intensity	9.39	1.69
H_2 diagonal		
ω_e	2858	2834
intensity	28.37	4.32
(9,0) Tube		
H_2 horizontal		
ω_e	2880	2854
intensity	32.17	5.27
H_2 diagonal		
ω_e	2858	2834
intensity	28.38	4.34

The bands in NH_3 are quite strong and could potentially contribute to the IR spectra if it was physisorbed on the carbon nanotubes. However, as noted above, no bands are observed when the plasma is not turned on, and therefore we do not consider physisorbed species further.

Table 2 summarizes the results for two H atoms on the sides of the tubes. For the (9,0) tube the two orientations differ by 2.4 kcal/mol, while for the (5,5) the diagonal is 10.3 kcal/mol more stable than the vertical. The C−H stretching frequencies range from 2834 to 2928 cm^{-1}, depending on the tube and the orientation. Previous experiments[2] show the C−H stretching band to be about 100 cm^{-1} wide with two components, one centered at 2920 cm^{-1} and the other at 2950 cm^{-1}. Considering that we have only taken two sites on two different tubes, the agreement with experiment is good and supports the use of a simple model for the vibrational frequencies of the NH_n species.

We consider NH_2, both as a single NH_2 on the surface and with a neighboring H atom. For the H + NH_2 species on the (5,5) tube, the diagonal is 8.3 kcal/mol more stable than the vertical, which is similar to the case of two H atoms. For both the (5,5) and (9,0) tubes, the NH_2 is bound by about 20 kcal/mol less than the hydrogen atom. The smaller binding plus the fact that NH_2 will probably react only when it hits the tube with the nitrogen end, while an H atom has no such geometrical restriction on reaction, means that the reaction rate for H atoms with the surface is probably larger than for the NH_2 radicals.

Table 3 summarizes the computed vibrational frequencies for the NH_2 species. Excluding the wagging motion, the addition of the neighboring H atom has only a very small effect on the NH_2 frequencies. The N−H stretching frequencies vary from 3183 to 3347 cm^{-1} depending on the tube, the orientation, and whether there is a neighboring H atom. This frequency range falls between the N−H stretching modes in NH_2 and the intense band in NH_3; thus, these stretches appear to be in an unobstructed region of the spectra. Unfortunately, all of the N−H stretches are rather weak. The H−N−H bending mode shows a rather narrow frequency range, 1624−1647 cm^{-1}, and has a sizable intensity. Finally we note that the C−H stretching frequencies are similar to those obtained for the H-only case discussed above, although the C−H stretching intensities in the H + NH_2 cases are smaller than in the pure H cases.

TABLE 3: Summary of the Computed Vibrational Frequencies (cm^{-1}) and IR Intensities (km/mol) for NH_n on the (9,0) and (5,5) Tubes

	N−H s-stretch	N−H a-stretch	C−H stretch	H−N−H bend	wag
NH_2 (5,5)					
ω_e	3204	3322		1633	645
intensity	0.35	0.83		26.29	50.13
NH_2 + H diagonal (5,5)[a]					
ω_e	3211	3323	2841	1638	721
intensity	0.78	1.08	0.31	57.18	3.21
NH_2 + H vertical (5,5)					
ω_e	3183	3296	2834	1642	768
ω_e (ND_2 + D)	2296	2432	2079	1201	
intensity	1.09	0.39	1.07	37.19	58.51
NH_2 (9,0)					
ω_e	3219	3340		1624	662
intensity	0.49	1.17		31.69	26.76
NH_2 + H horizontal (9,0)					
ω_e	3231	3347	2883	1647	713
ω_e (ND_2 + D)	2325	2455	2117	1219	
intensity	0.65	2.18	1.95	41.18	137.14

[a] The results for a local minima that is slightly higher in energy are 3241, 3363, 2826, and 1628 cm^{-1} for the two N−H stretches, the C−H stretch, and the H−N−H bend, respectively. It was not possible to unambiguously identify the wag for the higher energy solution.

TABLE 4: Summary of the Computed N−H Stretching Frequencies (cm^{-1}) and IR Intensities (km/mol) for NH on the (9,9) and (5,5) Tubes[a]

	NH diagonal	NH vertical
(5,5)		
binding energy	22.0	65.0
ω_e	3142	3238
intensity	2.37	7.78
	NH diagonal	**NH horizontal**
(9,0)		
binding energy	24.3	7.9
ω_e	3235	3140
intensity	2.62	2.87

[a] The tube−NH binding energy (kcal/mol) is also given.

Unlike the H or NH_2 that bonds to one carbon atom, NH forms a bridge between two carbon atoms. For the (9,0) diagonal and (5,5) vertical sites, the formation of the C−N bonds breaks the C−C bond, while for the (9,0) horizontal and (5,5) diagonal sites, the C−C bond remains intact. Unlike most of the species studied, the NH binding energy varies significantly with tube and site (see Table 4). It would be very interesting to see the tube−NH binding energies computed using a better model, for example, one that includes a complete ring of tube carbon atoms and has periodic boundary conditions. However, N−H stretching modes are very local in nature, and our present model should be sufficiently accurate for the determination of the frequencies and IR intensities.

Table 4 summarizes the vibrational frequencies obtained for NH bonded to the (5,5) and (9,0) tubes. The cases where the C−C bond is broken have an N−H stretching frequency that is

TABLE 5: Assignment of IR Bands Observed after NH_3 and ND_3 Microwave Plasma Discharges on SWNT

		expt					
freq (cm^{-1})	assignment	20 min NH_3	40 min NH_3	20 min ND_3	40 min ND_3	210 min ND_3	ref
3343	N−H stretching	×	×	×	×		11, 12
3268	N−H stretching?					x	11, 12
3200−3190	N−H stretching	×	×	×	×		11, 12
2530	N−D stretching					×	11, 12
2210, 2110	C−D stretching			×	×	×	2, 12
1670−1668	C═N, H−N−H bending	×	×	×	×	×	11, 12
1584−1560	C═C, C═N	×	×	×	×	×	11, 12, 14
2181, 2153[a]	C≡N						11,12

[a] These bands are observed just after 1 min of NH_3 discharge in the RF inductively coupled plasma operated at 25 W. For ND_3 discharge in the same configuration, a band at 2150 cm^{-1} is convoluted within the band structure assigned to C−D stretching.

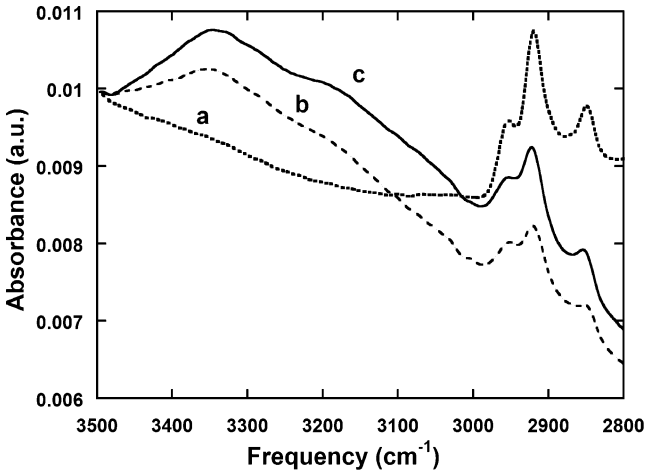

Figure 3. FTIR spectra (2800−3500 cm^{-1}) of SWNT after exposure to NH_3 microwave plasma: (a) SWNT on CaF_2 substrate after heating; (b) after 20 min of plasma exposure; (c) after 40 min of exposure. C−H bands are clearly evident.

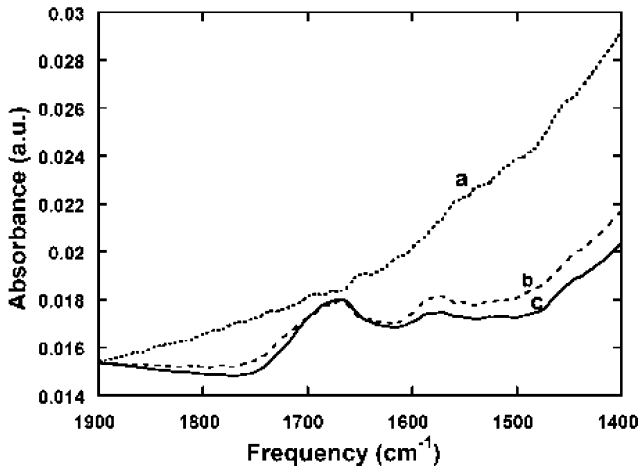

Figure 4. FTIR spectra (1400−1900 cm^{-1}) of SWNT after exposure to NH_3 microwave plasma: (a) SWNT on CaF_2 substrate after heating; (b) after 20 min of plasma exposure; (c) after 40 min of exposure.

about 100 cm^{-1} larger than those where the C−C bond is intact. While the N−H stretch is stronger than those obtained for tube−NH_2, it does have some overlap with the N−H stretch in the tube−NH_2 system, and it is therefore difficult to separate NH from NH_2 functionalization based on the N−H stretches. The other bands for the tube−NH case are not easy to identify, as they are mixed with tube C−C motions and/or with link−H motions, and are therefore not reported.

V. Experimental Results and Discussion

1. FTIR Spectroscopy. A Thermo Nicolet Nexus 670 FTIR at 4 cm^{-1} resolution was used in this study. Evidence of functionalization by NH_3 microwave plasma discharge is found just after 20 min of discharge by the formation of peaks in expected regions corresponding to N−H stretching and bending of primary and secondary amines,[11,12] C═N[11,12] type bonds, and/or C═C[11,12] (Figures 3 and 4). Further evidence is supplied by fluctuations of the peaks around 2900 cm^{-1} corresponding to C−H bonding;[2] hydrogen initially bonded to the walls of the SWNTs were being displaced in favor of the species produced in the plasma. After 20 min of discharge there is a decrease in the intensities of C−H bands, while an increase is observed after 40 min of discharge. We assume that, at longer times, the more reactive H atoms are preferentially reacting with the SWNTs surface. IR spectroscopy revealed features around 3343, 3198, 1670, and 1571 cm^{-1} upon functionalization of SWNTs with ammonia. Assignments of IR bands are tabulated in Table 5. N-H type stretching is observed around 3343 and 3198 cm^{-1}. These bands are consistent with the computed values for the N−H symmetric and asymmetric stretches in tube−NH_2, with some contribution from the tube−NH systems.

Hamon et al.[13] functionalized the ends of open metallic SWNT with CONH-4-$C_6H_4(CH_2)_{13}CH_3$. Their IR spectrum shows an N−H stretching frequency of 3450 cm^{-1}, which corresponds to an NH in the side chain, not the N atom bonded directly to the tube. Since our N−H stretching bands are at much lower frequency, we believe it is reasonable to rule out the reaction of NH_3 fragments with some molecules linked to the SWNT wall, but rather they have reacted with the side walls.

It is possible to assign the band around 1670 cm^{-1} as C═N and/or to H−N−H bending. On the basis of computed results, it seems likely that the band corresponds to the H−N−H bend. The peak around 1571 cm^{-1} is assigned to C═C and/or C═N. A similar peak was observed at 1560 cm^{-1} through FTIR spectroscopy by Zheng et al.[14] after 60 keV N ion implantation into diamond. Sinyashin et al.[15] have reported C═N frequency at 1572 cm^{-1} for fullerenes with surface functionalities produced by the reaction with phosphoryl nitrile oxide. Observation of IR bands below 1500 cm^{-1} is greatly hampered by the sloping increase of the substrate absorbance.

Similar IR band structures were obtained using deuterated ammonia, with the addition of C−D type stretching bands.[1] Expected decrease in the C−H bonding on the SWNTs surface is consistent with a decrease in band intensities around 2900 cm^{-1}, in favor of the species produced in the plasma. N−H type stretching bands are made possible by the abundance of nitrogen through the discharge and hydrogen contained in the SWNTs and regular ammonia impurities contained in the gas cylinder. IR bands appear around 3334 (N−H), 3195 (N−H),

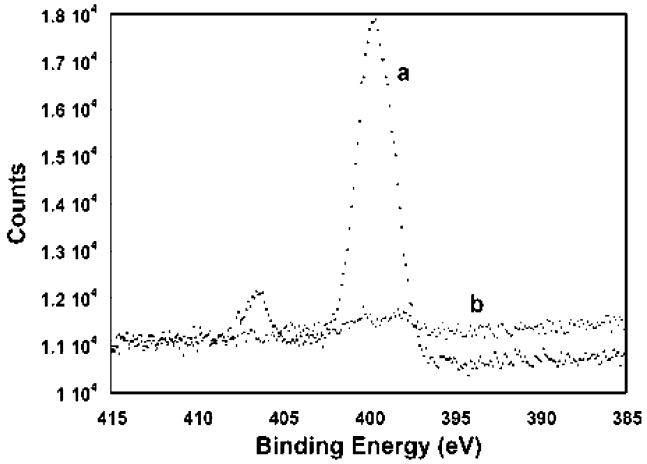

Figure 5. Nitrogen region of the XPS spectra of SWNTs: (a) functionalized and (b) unfunctionalized. Spectrum shows at least two nitrogen peaks after functionalization. The peak at 399.5 eV is likely due to amine. The second nitrogen peak at 406.4 eV is consistent with nitrogen−oxygen bonding.

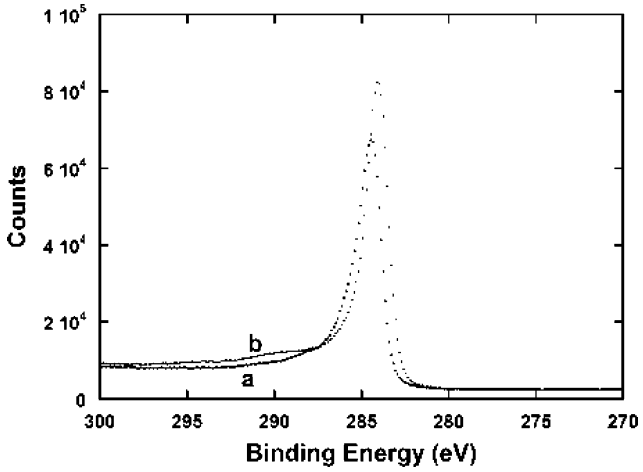

Figure 6. Carbon region of the XPS spectra of SWNTs: (a) functionalized and (b) unfunctionalized. A shift in higher binding energy is apparent upon functionalization.

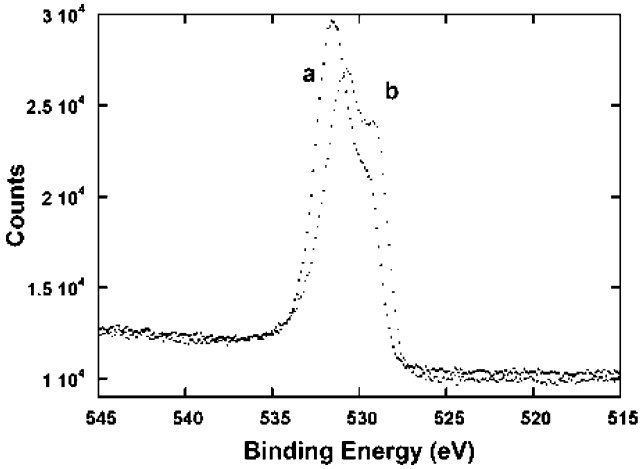

Figure 7. Oxygen region of the XPS spectra of SWNTs: (a) functionalized and (b) unfunctionalized. The main peak shifts toward higher energy after functionalization, indicating a decrease in carbon−oxygen bonding relative to carbon−nitrogen bonding.

2210 (C−D), 2110 (C−D), 1668 (C═N, H−N−H), and 1566 cm^{-1} (C═C, C═N).

A peak around 2530 cm^{-1} appears after 3.5 h of discharge and is assignable to N−D stretching. Such an extended exposure also etches away SWNTs from the substrate surface leaving a thin film of yellowish appearance. The structure previously assigned to N−H type stretching evolves into a broad peak centered on 3270 cm^{-1}. A peak at 1430 cm^{-1} is also formed after this extended exposure, but there are no conclusive data regarding its assignment.

It is important to note that samples have been exposed to air throughout the transitional stages of the experiments (e.g., moving samples from the furnace to spectrometer and to the vacuum system). However, no oxidization problems have been experienced with previous work with functionalized SWNTs,[1,2] and, therefore, the IR bands reported in this paper are assigned neglecting any role of oxidation. XPS shows evidence of oxygen though, however, in smaller amounts than the functionalities discussed in this section. Thus, we believe any oxygenated compounds present on the SWNT surfaces do not alter IR absorptions sufficiently, allowing the spectral assignment to remain coherent with the computed results. Ammonia-functionalized SWNTs are expected to have increased solubility in water and might make them reactive to atomic or molecular species in air. Zheng et al.[14] reported N−O type bonding on the surface layers of diamond films. C−O and O−H type bonding have been reported on SWNT surface producing IR spectral features differentiable from those observed in this experiment.[16] Amide bonds have also been reported with C═O bands at 1663 and 1642 cm^{-1}, but no assignment for C−N bonding or N−H stretching in IR.[13,17] The first of these bands (1663 cm^{-1}) has a value similar to the one reported in this paper and the second (1642 cm^{-1}) is not observed.

2. X-ray Photoelectron Spectroscopy. The XPS spectra of the NH_3 plasma-exposed samples indicate the incorporation of at least two types of nitrogen functional groups on the SWNT (Figure 5). A significant increase in nitrogen content was observed on the surface of the plasma-exposed SWNT compared to the control sample. For the control, the relative atom percent of C, N, and O was 88.1, 0.4, and 11.5, respectively, while for the NH_3 plasma-exposed sample, these values were 81.5% C, 6.6% N, and 11.9% O. A nitrogen (1s) peak at 399.5 eV is indicative of nitrogen carbon bonding, which can be assigned to amine and (possibly) nitrile functional groups in different chemical environments. The latter assignment could be discarded by the absence of IR bands in the nitrile regions. (We have observed nitrile-specific IR bands when the SWNT samples are submerged in a radio frequency inductively coupled plasma (ICP) 20 of NH_3. In fact, the appearance of this band led us to abandon the ICP source since such a band is an indication that the integrity of the nanotube structure is affected significantly. In our ICP setup, the sample is unprotected from radiation and remains exposed to more energetic plasma species; thus, we believe it is not appropriate for sidewall functionalization.) A second nitrogen peak at 406.4 eV is consistent with nitrogen−oxygen bonding. The ratio of the carbon−nitrogen bonding (339.5 eV) to nitrogen−oxygen bonding (406.4 eV) in the plasma-exposed sample is approximately 10:1. Support of these assignments and further evidence of functionalization can be seen in the carbon and oxygen regions of the XPS spectra. The carbon peak for both the functionalized and unfunctionalized SWNT can be resolved into multiple peaks. A shift to high binding energy is seen for the main carbon peak in the functionalized (284.4 eV) sample compared to the unfunctionalized sample (284.1 eV), indicating an increase in functionalization at the surface of the SWNT as a result of plasma exposure (Figure 6). In the oxygen region, of the functionalized sample (Figure 7), the main oxygen peak is shifted to higher

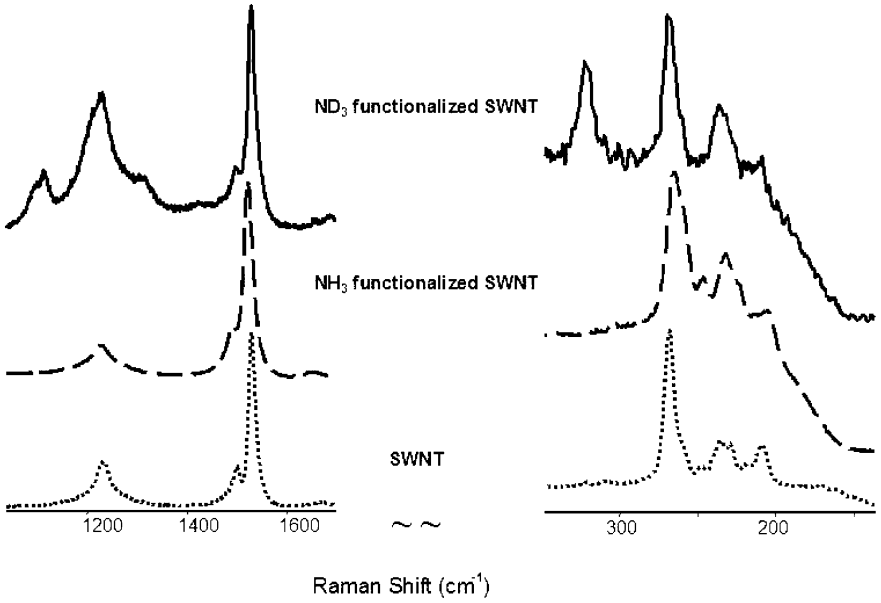

Figure 8. Raman spectra analyses. These show the high-frequency RBM (267, 241, 232, 208, and 172 cm^{-1} in the pristine SWNT) decreases, indicating the percentage of smaller diameters decreases as likely the functionalized nanotubes. The frequency of the G-band (1594 cm^{-1} in pristine SWNT) in the TM region shifts toward the higher energy (1583 cm^{-1} in the NH_3 functionalized SWNT), and line shape is broadened, correlating with the SWNT side-wall functionalizations.

binding energy, indicating a decrease in carbon−oxygen bonding relative to carbon−nitrogen bonding as a result of NH_3 plasma exposure.

3. Raman Spectroscopy. As previous studies show,[18,19] below 500 cm^{-1}, the frequency of the radial breathing modes (RBM) is inversely proportional to the SWNT diameter. SWNTs exposed to both NH_3 discharges display RBM frequency shifts from that of the pristine nanotubes (Figure 8). In both cases, the percentage of smaller diameter nanotubes (0.9 nm for example) decreases since the nanotubes are functionalized. The tangential modes (TM) between 1100 and 1800 cm^{-1} display the following behavior for both NH_3 and ND_3 precursors. The frequency of the G-band (1594 cm^{-1} in pristine SWNT) shifts toward the lower energy (1583 cm^{-1} in the NH_3 functionalized SWNT), and the line shape is broadened. This change in G-band frequency strongly suggests the sidewall interactions with NH species. In the case of ND_3 discharge additional TM features are seen, possibly due to the multiple interactions from different ND_x species, or different reaction sites as the theoretical calculations show. Another interesting Raman observation in the TM region is that the intensity of sp^3 carbon increases in the ND_3 functionalized SWNTs, while this intensity in the case of NH_3 functionalized SWNTs decreases. As sidewall defect sites, sp^3 carbon often acts as an active site for functionalization. The observed sp^3 intensity charge is consistent with the decrease in D-band intensity for SWNTs exposed to NH_3 discharge from that of pristine SWNTs, whereas the D-band intensity increases for ND_3-exposed SWNTs. The observed shift of the band at 1553 to 1563 cm^{-1} for NH_3-exposed nanotubes also suggests functionalization; however, a similar change does not occur with ND_3. The increase in the relative intensity ratio of sp^3 to sp^2 carbon from ND_3-functionalized SWNTs compared to pristine SWNTs suggests ND and ND_2 coexist on the SWNT sidewall. To summarize, combined RBM relative intensity and TM frequency and line shape changes, strongly suggest the SWNT functionalization through microwave discharge.

VI. Conclusions

A cold plasma approach has been used to functionalize single-wall carbon nanotubes using an ammonia discharge. FTIR spectroscopy has been used to characterize the functionalized SWNT samples. Characteristic peaks corresponding to tube−H and N−H stretches and the H−N−H bend have been observed, and the assignments of these bands agree well with computational modeling results also presented here. The data from XPS and Raman analysis also support this assignment. Whereas discharges of molecular gases allow functionalization of a single desirable species (such as H, C1, or F), discharges of ammonia and other such gases often produce a host of active radicals. For functionalization of a selective group from such precursors, the discharge output can be subjected to a mass diffraction just as used in common mass spectroscopy, to pick and choose the species of interest, which can be directed toward the SWNT sample. Thus, the glow-discharge process provides a clear and efficient approach to functionalize nanotubes with any chemical group as long as a suitable precursor to strike a cold plasma is available.

Acknowledgment. B.N.K, R.C.Q., and H.I. are employed by SETI Institute, and C.R.S. (summer intern from University of Washington) and B.C. were employed by Eloret Corp., and their work was supported by NASA contracts to the respective organizations. Professor Richard Smalley and his HiPCO team are acknowledged for providing the SWNTs.

References and Notes

(1) Khare, B. N.; Meyyappan, M.; Cassell, A. M.; Nguyen, C. V.; Han, J. *Nano Lett.* **2002**, *2*, 73.

(2) Khare, B. N.; Meyyappan, M.; Kralj, J.; Wilhite, P.; Sisay, M.; Imanaka, H.; Koehne, J.; Bauschlicher, C. W. *Appl. Phys. Lett.* **2002**, *81*, 5237.

(3) Svensson, M.; Humbel, S.; Froese, R. D. J.; Matsubara, T.; Sieber, S.; Morokuma, K. *J. Phys. Chem.* **1996**, *100*, 19357.

(4) Becke, A. D. *J. Chem. Phys.* **1993**, *98*, 5648.

(5) Stephens, P. J.; Devlin, F. J.; Chabalowski, C. F.; Frisch, M. J. *J. Phys. Chem.* **1994**, *98*, 11623.

(6) Frisch, M. J.; Pople, J. A.; Binkley, J. S. *J. Chem. Phys.* **1984**, *80*, 3265, and references therein.

(7) Rappe, A. K.; Casewit, C. J.; Colwell, K. S.; Goddard, W. A.; Skiff, W. M. *J. Am. Chem. Soc.* **1992**, *114*, 10024.

(8) Frisch, M. J.; et al. *Gaussian 98*, Revision A.11; Gaussian, Inc.: Pittsburgh, PA, 1998.

(9) Flukiger, P.; Luthi, H. P.; Portmann, S.; Weber, J. *MOLEKEL 4.2*; Swiss Center for Scientic Computing: Manno, Switzerland, 2000−2002. Portmann, S.; Luthi, H. P. *Chimia* **2000**, *54*, 766.

(10) Bauschlicher, C. W.; Langhoff, S. R. *Spectrochim. Acta, Part A* **1997**, *53*, 1225.

(11) Szymanski, H.; Erickson, R. *Infrared Band Handbook*, 2nd ed.; IFI/Plenum: New York−Washington−London, 1970.

(12) Socrates, G. *Infrared and Raman Characteristic Group frequencies. Tables and Charts*, 3rd ed.; Wiley: Chichester−New York−Weinheim−Toronto−Brisbane−Singapore, 2001.

(13) Hamon, M. A.; Chen, J.; Hu, H.; Chen, Y.; Itkis, M. E.; Rao, A. M.; Eklund, P. C.; Haddon, R. C. *Adv. Mater.* **1999**, *11*, 834.

(14) Zheng, W. T.; Cao, P. J.; Li, J. J.; Wang, X.; Jin, Z. S. *Surf. Coat. Technol.* **2003**, *173*, 213.

(15) Sinyashin, O. G.; Romanova, I. P.; Sagitova, F. R.; Pavlov, V. A.; Kovalenko, V. I.; Badev, Y. V.; Azancheev, N. M.; Ilyasov, V.; Chernova, A. V.; Vandyukova, I. I. *Mendeleev Commun.* **1998**, *2*, 43.

(16) Kuznetsova, A.; Mawhinney, D. B.; Naumenko, V.; Yates, J. T.; Liu, J.; Smalley, R. E. *Chem. Phys. Lett.* **2000**, *321*, 292.

(17) Chen, J.; Hamon, M. A.; Hu, H.; Chen, Y.; Rao, A. M.; Eklund, P. C.; Haddon, R. C. *Science* **1998**, *282*, 95.

(18) Chen, B.; Parker, G., II; Han, J.; Meyyappan, M.; Cassell, A. M. *Chem. Mater.* **2002**, *14*, 1891.

(19) Jorio, A.; Saito, R.; Hafner, J. H.; Lieber, C. M.; Hunter, M.; McClure, T.; Dresselhaus, G.; Dresselhaus, M. S. *Phys. Rev. Lett.* **2001**, *86*, 1118.